Direct Evidence of Conformational Changes Associated with Voltage Gating in a Voltage Sensor Protein by Time-Resolved X-ray/Neutron Interferometry

Andrey Y. Tronin,[†] C. Erik Nordgren,[†] Joseph W. Strzalka,[‡] Ivan Kuzmenko,[‡] David L. Worcester,[§] Valeria Lauter,[∥] J. Alfredo Freites,[⊥] Douglas J. Tobias,[⊥] and J. Kent Blasie*,[†]

[†]Department of Chemistry, University of Pennsylvania, Philadelphia, Pennsylvania 19104, United States

[‡]X-ray Science Division, Advanced Photon Source, Argonne National Laboratory, Argonne, Illinois 60439, United States

[§]Department of Physiology & Biophysics, University of California Irvine, Irvine, California 92697, United States

[∥]Spallation Neutron Source, Oak Ridge National Laboratory, Oak Ridge, Tennessee 37831, United States

[⊥]Department of Chemistry, University of California Irvine, Irvine, California 92697, United States

S *Supporting Information*

ABSTRACT: The voltage sensor domain (VSD) of voltage-gated cation (e.g., Na^+, K^+) channels central to neurological signal transmission can function as a distinct module. When linked to an otherwise voltage-insensitive, ion-selective membrane pore, the VSD imparts voltage sensitivity to the channel. Proteins homologous with the VSD have recently been found to function themselves as voltage-gated proton channels or to impart voltage sensitivity to enzymes. Determining the conformational changes associated with voltage gating in the VSD itself in the absence of a pore domain thereby gains importance. We report the direct measurement of changes in the scattering-length density (SLD) profile of the VSD protein, vectorially oriented within a reconstituted phospholipid bilayer membrane, as a function of the transmembrane electric potential by time-resolved X-ray and neutron interferometry. The changes in the experimental SLD profiles for both polarizing and depolarizing potentials with respect to zero potential were found to extend over the entire length of the isolated VSD's profile structure. The characteristics of the changes observed were in qualitative agreement with molecular dynamics simulations of a related membrane system, suggesting an initial interpretation of these changes in terms of the VSD's atomic-level 3-D structure.
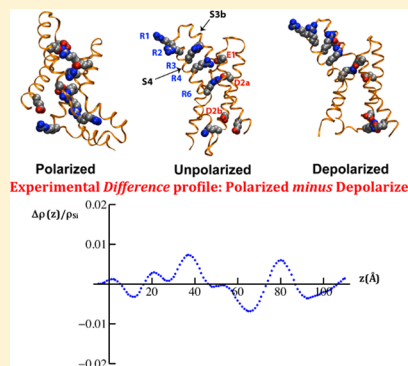
INTRODUCTION

Voltage-gated cation (e.g., Na^+, K^+) channels are central to neurological signal transmission.[1,2] X-ray crystal structures of the open state of several voltage-gated potassium (Kv) channels[3,4] and a sodium (Nav) channel have recently been determined.[5] Kv channels are composed of four identical subunits, each containing a voltage-sensor domain (VSD) and one-fourth of the pore domain (PD), the latter forming the complete pore in the homotetrameric channel. Despite numerous experimental and computational studies, the mechanism of voltage gating, namely the coupling of specific conformational changes within the VSD in response to depolarizing potentials with respect to the resting transmembrane electric potential, to opening the PD resulting in transmembrane ionic current, has not been fully resolved for two reasons. One arises because the direct methods utilized for the investigation of the 3-D structure of either the detergent solubilized VSD (e.g., X-ray crystallography[6] and solution NMR[7]) or the complete Kv/Nav channel (e.g., X-ray crystallography[3−5]) cannot provide the structure as a function of the membrane potential in the absence of the membrane, the

closed form of the complete channel occurring only at the resting potential. Another arises because the physical−chemical techniques utilized to investigate the structures of the complete Kv/Nav channel in the membrane as a function of the potential have been more indirect. Because they generally utilize site-directed mutation of one or two residues at a time within the VSD to cysteine, followed by either their labeling with large chromophores for the purpose of fluorescence or light-energy transfer measurements [e.g., refs 8 and 9] or alternatively for measuring their accessibility to lipid soluble or insoluble reagents [e.g., refs 10 and 11], as a function of the transmembrane electric potential, they are likely to involve some perturbation of the structure and dynamics of the protein and/or its membrane environment.

The VSD itself can be considered as a distinct module that, when linked to an otherwise voltage-insensitive, ion-selective membrane pore, imparts voltage sensitivity to the channel.[12] Furthermore, voltage-sensor proteins homologous with the
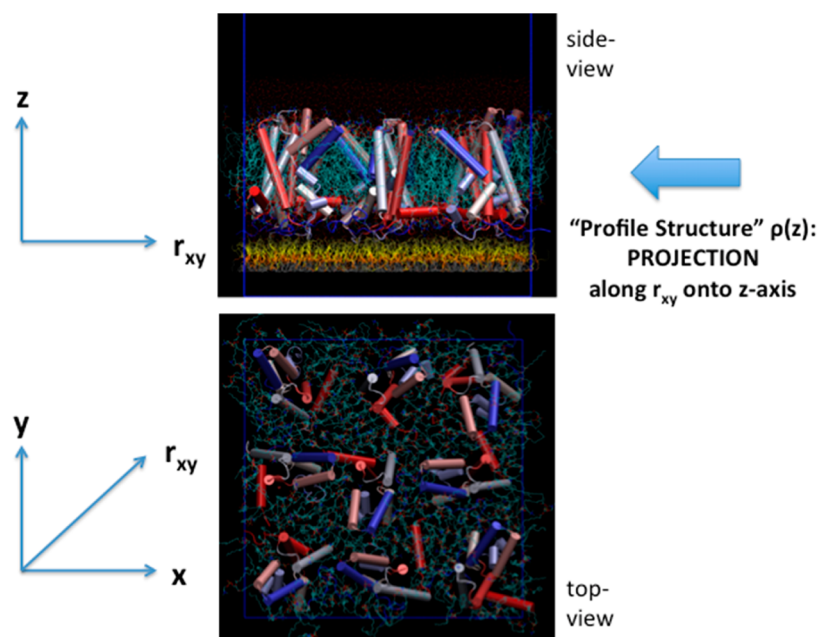
Figure 1. Molecular graphics representation of a small 3 × 3 ensemble of the vectorially oriented VSD molecules (α-helices represented as solid cylinders) solvated by a POPC bilayer (turquoise) tethered to the surface of a solid inorganic substrate (not shown) below the monolayer of tethering chain molecules (yellow) in the side view. The "profile structure" arises from the projection of the 3-D structure of the membrane along $\mathbf{r}_{xy}$ vectors parallel to the plane onto the z-axis normal to the plane of the membrane. The VSD molecules have been rotated randomly with respect to one another about the z-axis in the top view. However, unlike in the top view shown, experimentally, the VSD's exhibit only glass-like order in the x–y plane, even at this low average area/VSD of ~1400 Å^2 approximating that of the experimental situation.

VSD have recently been found to function themselves as voltage-gated proton channels involved in pH regulation during phagocytosis[13] or to impart voltage sensitivity to enzymes involved in signaling.[14] As for the complete Kv/Nav channels, emerging X-ray crystal structures[15,16] for these proteins cannot directly address their membrane potential-dependent conformational states. Thus, elucidating the conformational states associated with voltage gating within the VSD itself, and these homologous voltage-sensor proteins, gains broad biological significance, especially utilizing approaches that minimize any perturbation of the structure and dynamics of either the protein itself or its membrane environment.

We have developed a single membrane system containing the vectorially oriented VSD, or the complete Kv/Nav channel, at high in-plane density tethered to the surface of a solid inorganic substrate,[17] as illustrated in Figure 1. Two different methods were utilized to fabricate the single membrane on the surface of the substrate: one referred to as "self-assembly" and the other as "directed assembly". Although published previously, the methods are briefly summarized in the Experimental Methods section and illustrated with figures in the Supporting Information. When placed in a suitable electrochemical cell, the so-called "profile structure" of the membrane can be investigated using the direct methods of high energy X-ray reflectivity and neutron reflectivity, each enhanced by utilizing an interferometric technique enabled by the fabrication of an inorganic multilayer structure on the surface of the substrate to which the membrane is tethered.[17−19] "Profile" refers to the projection of the membrane's 3-D structure dominated by the VSD protein, parallel to the plane onto the axis normal to the plane of the membrane, as also illustrated in Figure 1. For X-rays, this projected structure is the X-ray scattering length (or electron) density profile (denoted herein as the xSLD profile) and for neutrons the neutron scattering length density profile

(similarly denoted as the nSLD profile). The significance of the X-ray (or neutron) interferometric technique was clearly demonstrated in an earlier publication[18] via a direct comparison of the X-ray reflectivity from a Langmuir monolayer of an amphiphilic 4-helix bundle protein at the water−air interface in the absence and presence of the interferometric effect. The technique is briefly summarized in the Experimental Methods and illustrated with figures in the Supporting Information using this example.

The profile structure of this single membrane system has been extensively characterized by neutron interferometry.[19] This characterization is in full agreement with the independent, but more limited results from X-ray interferometry.[17] Importantly, it demonstrated several key elements essential for the success of the approach utilized in this work. With reference to Figure S1 in the Supporting Information (from ref 19), the VSD protein exhibits a unidirectional vectorial orientation in the membrane, the in-plane density of the protein is sufficiently high so that the protein dominates the profile structure with the protein occupying ~50% of the membrane area, the space between adjacent protein molecules in the membrane plane is filled by an asymmetric phospholipid bilayer occupying the remaining ~50% of the membrane area, the layer containing the chain molecules tethering the membrane to the inorganic surface positions the membrane ~20 Å away from the inorganic surface, and the surface of the membrane proximal to the inorganic surface is highly hydrated to the level of ~50% that of bulk water, the distal surface being fully hydrated.

In this work, we report the characterization of the electrical properties of this single membrane system via electrical impedance spectroscopy. These properties (resistance and capacitance) were found sufficient to permit the direct measurement of changes in the SLD profiles of the VSD

protein, vectorially oriented within the single phospholipid bilayer membrane, as a function of the steady-state transmembrane electric potential. A time-resolved version of the direct methods of X-ray and neutron interferometry was utilized, analogous to the classic "pump-probe" approach widely applied using spectroscopic techniques. The transmembrane potential was varied in a stepwise, cyclic fashion with data collection at each of three values of the potential. For the X-ray case, only one cycle was sufficient to achieve satisfactory standard errors at each value of the potential due to the high photon flux density available with the synchrotron X-ray source, although four cycles of data were collected and analyzed separately. With the much lower flux density of neutrons from the spallation neutron source, the data were necessarily averaged over many cycles for each value of the potential to reduce the standard errors prior to further data reduction and analysis. This approach for each case was employed to ensure that the changes in the SLD profiles detected were fully reversible and to avoid the possibility of trapping the VSD in an inactive state by exposing the protein to a particular potential for an extended time. The changes in the experimental SLD profiles so observed were found to be qualitatively consistent with the results from molecular dynamics simulations of a related membrane system, thus suggesting an initial interpretation of these changes in terms of the VSD's atomic-level 3-D structure.

■ EXPERIMENTAL METHODS

Fabrication of the Reconstituted VSD:POPC Membrane. Two different methods, designated as "self-assembly" and "directed assembly" and described previously,[17] were used for the preparation of single membranes tethered to the surface of an inorganic SiGeSi or SiNiSi multilayer substrate, the membrane composed of a phospholipid bilayer (POPC; 1-palmitoyl-2-oleoyl-sn-glycero-3-phosphocholine) containing the voltage sensing domain (VSD) of the voltage-gated potassium channel from *Arepyrum pernix* KvAP, vectorially oriented with respect to the normal to the membrane plane at high in-plane surface density.[17] They are briefly summarized in the Supporting Information. Importantly, VSD:POPC membranes formed by both the SA and DA methods were investigated in this work.

Fabrication of the Hybrid OTS:POPC Bilayer. The hybrid bilayer was formed via the chemisorption of OTS (octadecyltrichlorosilane) onto the silicon oxide surface of a SiGeSi multilayer substrate. A monolayer of POPC (1-palmitoyl-2-oleoyl-sn-glycero-3-phosphocholine) was physisorbed onto the hydrophobic surface of the substrate alkylated with the OTS via the rapid solvent-exchange technique.[20]

Electrical Properties of the Reconstituted VSD:POPC Membranes and the Hybrid OTS:POPC Bilayers. The electrochemical cells employed in the X-ray and neutron interferometry experiments are substantially different for each of the two scattering techniques employed. As a result, they are fully described in their respective Data Collection sections below. Electrical impedance spectroscopy (EIS) measurements, using a CHI660D electrochemical workstation from CH Instruments, were performed *in situ* on the membrane specimens utilized in the X-ray and neutron interferometry experiments, as well as on many additional, entirely analogous specimens performed *ex situ*. These data were usually successfully modeled with simple equivalent circuits,[21] composed of a resistance, representing that of the silicon oxide surface of the Si−Ge−Si or Si−Ni−Si multilayer substrates, in series with an RC component, representing the bio-organic overlayer on its surface, e.g., the reconstituted VSD:POPC membrane or the hybrid OTS:POPC bilayer.

X-ray and Neutron Interferometry. Interferometry is a form of the specular X-ray or neutron reflectivity technique that enhances the

sensitivity to a bio-organic layer adjacent the surface of a solid inorganic multilayer substrate and allows the direct determination of the SLD profile for the bioinorganic layer.[17−19] It is briefly summarized in the Supporting Information.

X-ray Interferometry Data Collection as a Function of the Membrane Potential. The method for the collection of specular X-ray reflectivity data, enhanced by interferometry and corrected for the beam footprint on the specimen and off-specular reflectivity, from single membranes tethered to the surface of an inorganic multilayer substrate fully hydrated with an aqueous medium, utilizing synchrotron radiation from an undulator source at sufficiently high X-ray energy to penetrate the aqueous medium, has been described previously.[17] With X-rays, the inorganic substrate was a SiGeSi multilayer fabricated by magnetron sputtering onto heavily doped silicon. The electrochemical cell was formed by pressing the end of 1 cm diameter Kapton tubing against the surface of the substrate possessing the membrane; the area of the membrane exposed to the X-ray beam in front-side reflection geometry[19] was less than 0.1×1.0 cm^2 at grazing angles of incidence. The electrolyte was 100 mM KCl in 1 mM Tris buffer at pH 7.8. The substrate served as the working electrode held at ground potential and a platinum electrode in the electrolyte served as the counter electrode to which the potential was applied via a commercially available potentiostat, also allowing for *in situ* measurement of the electrical properties of the membrane via impedance spectroscopy. Specular X-ray reflectivity from the substrate:bio-organic overlayer system was collected in front-side geometry, utilizing a flat substrate and monochromatic radiation, performing a $\theta-2\theta$ scan to collect data over a range of momentum transfer perpendicular to the substrate surface, Q_z, where θ is the angle of X-ray incidence with respect to the plane of the substrate's surface possessing the overlayer and 2θ the angle of reflection with respect to the incident beam. Unlike highly penetrating neutrons, high-energy X-rays (e.g., >20 keV) are required to penetrate the aqueous medium hydrating the membrane within an electrochemical cell. Herein, "time resolution" is utilized only to denote the investigation of the profile structure of the VSD protein at selected values of the "steady-state" transmembrane potential as the potential is varied cyclically in a stepwise manner over multiple cycles during reflectivity data collection. An ensemble of VSDs is capable of responding to such a step in the potential on the time scale of a few milliseconds.[1] The cyclic variation provides a key check on reversibility while avoiding trapping the protein in an inactive conformational state. With the vastly greater X-ray flux from an undulator-based synchrotron X-ray source, only very short collection times of 5−20 s were required for the majority of the large number of angles of incidence employed with monochromatic radiation, the incident beam appropriately attenuated to satisfy the count-rate limitations of the scintillation detector and achieve the desired standard error in the reflectivity data with increasing angle. The potential was then cycled over the sequence of 0 mV, −100 mV, +100 mV, 0 mV for each angle of incidence, utilizing 5−20 s/potential with increasing angle. The entire $\theta-2\theta$ scan for one cycle over all four values of the potential required a total of 82 min. Although as many as four cycles were collected for a particular specimen, the data were recorded separately for each cycle without any averaging over multiple cycles because the standard errors achieved for each value of the potential within a cycle were sufficient. The values of the potentials indicated here and subsequently refer to the potentials applied to the electrodes. Impedance spectroscopy suggests that the actual transmembrane potentials are at least 50−70% of these values, the reduction due to the silicon oxide surface of the substrates as described in the Results section.

Neutron Interferometry Data Collection as a Function of the Membrane Potential. The method for the collection of specular neutron reflectivity data, enhanced by interferometry and corrected for the beam footprint on the specimen and off-specular reflectivity, from single membranes tethered to the surface of an inorganic multilayer substrate fully hydrated with an aqueous medium, utilizing a polychromatic, pulsed spallation neutron source, has been described previously.[19,22] For neutrons, the inorganic substrate was a SiNiSi multilayer fabricated by magnetron sputtering onto undoped silicon.

m100mV – 0mV (Depolarized – Unpolarized)

p100mV – 0mV (Polarized – Unpolarized)
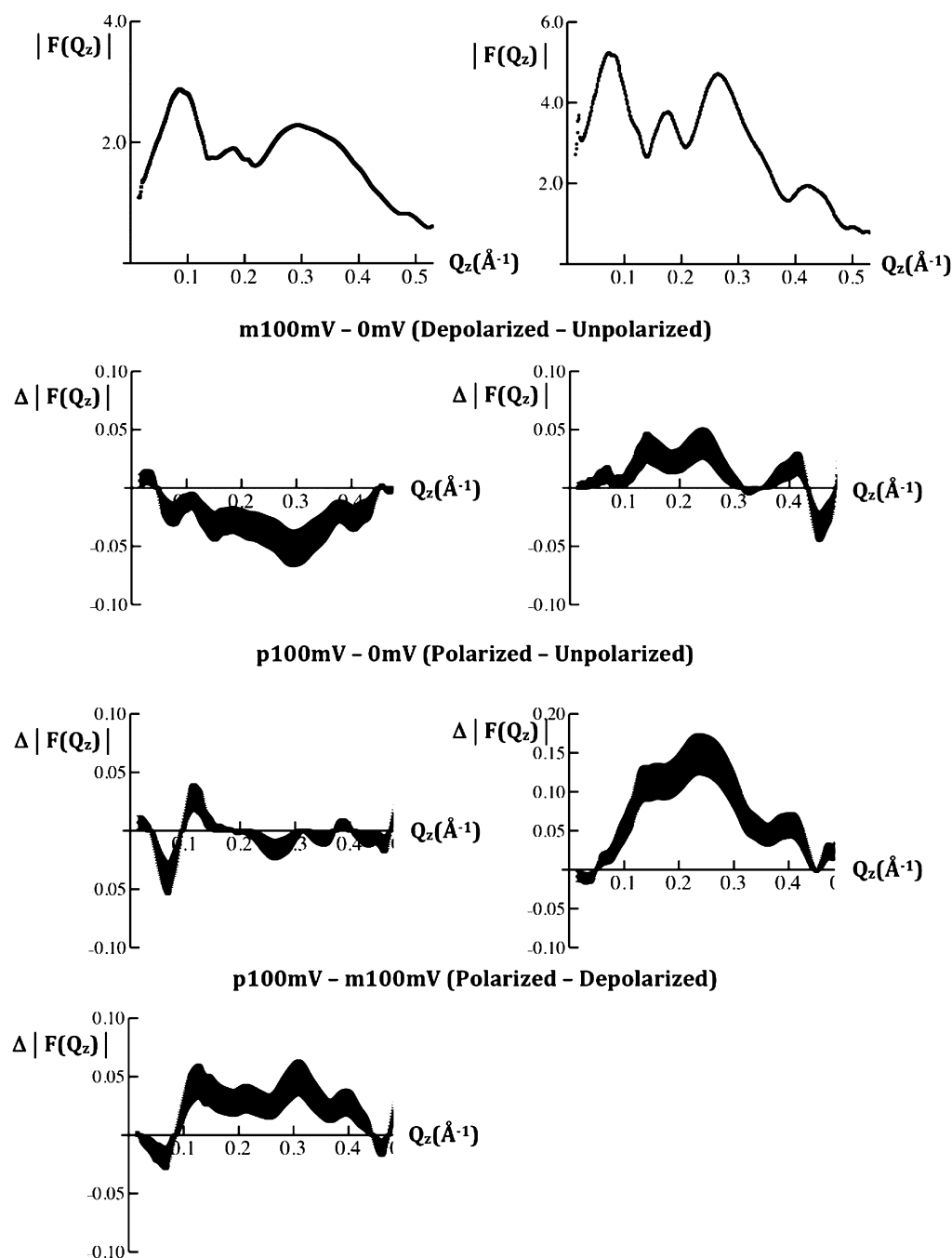

p100mV – m100mV (Polarized – Depolarized)

Figure 2. Left side: typical modulus $|F(Q_z)|$ data (top), calculated from the specular X-ray reflectivity $R(Q_z)/R_F(Q_z)$, where $|F(Q_z)|^2 = R(Q_z)/R_F(Q_z)$, for the VSD:POPC membrane tethered to the surface of a SiGeSi multilayer substrate at a transmembrane potential of 0 mV for the first two cycles of the series of potentials applied. The *difference* modulus data $\Delta|F(Q_z)|$ for the second cycle are shown in the panels below for the pairs of potentials indicated. Right side: typical modulus $|F(Q_z)|$ data (top) for the OTS:POPC hybrid bilayer tethered to the surface of a SiGeSi multilayer substrate at a transmembrane potential of 0 mV for the first two cycles of the series of potentials applied. The *difference* modulus data $\Delta|F(Q_z)|$ for the first cycle are shown in the panels below for the pairs of potentials indicated. The standard errors in the data are indicated for each case.

The electrochemical cell was formed between the surface of the substrate possessing the membrane and a silicon wafer separated by a nitrile gasket; the area of the membrane exposed to the incident neutron beam in backside geometry[19] was 1.0×4.0 cm^2 at grazing angles of incidence. The electrolyte was also 100 mM KCl in 1 mM Tris buffer at pH 7.8. Again, the substrate served as the working electrode held at ground potential, and a platinum electrode in the electrolyte served as the counter electrode to which the potential was applied. With the much lesser neutron flux from the spallation source, much longer collection times of 3−150 min were required for each of the few angles of incidence employing polychromatic radiation to achieve the desired standard error in the reflectivity data with increasing angle. Hence, the potential was cycled over the sequence of 0 mV, +100 mV, −100 mV, 0 mV for many cycles at each angle of incidence, utilizing 20 s/potential, and the data for each potential were summed prior to any further data reduction and analysis. The values of the potentials indicated here and subsequently again refer to the potentials applied to the electrodes. Impedance spectroscopy suggests that the actual transmembrane potentials are also at least 50−70% of these values, the reduction due to the silicon oxide surface of the substrates, as described in the Results section.
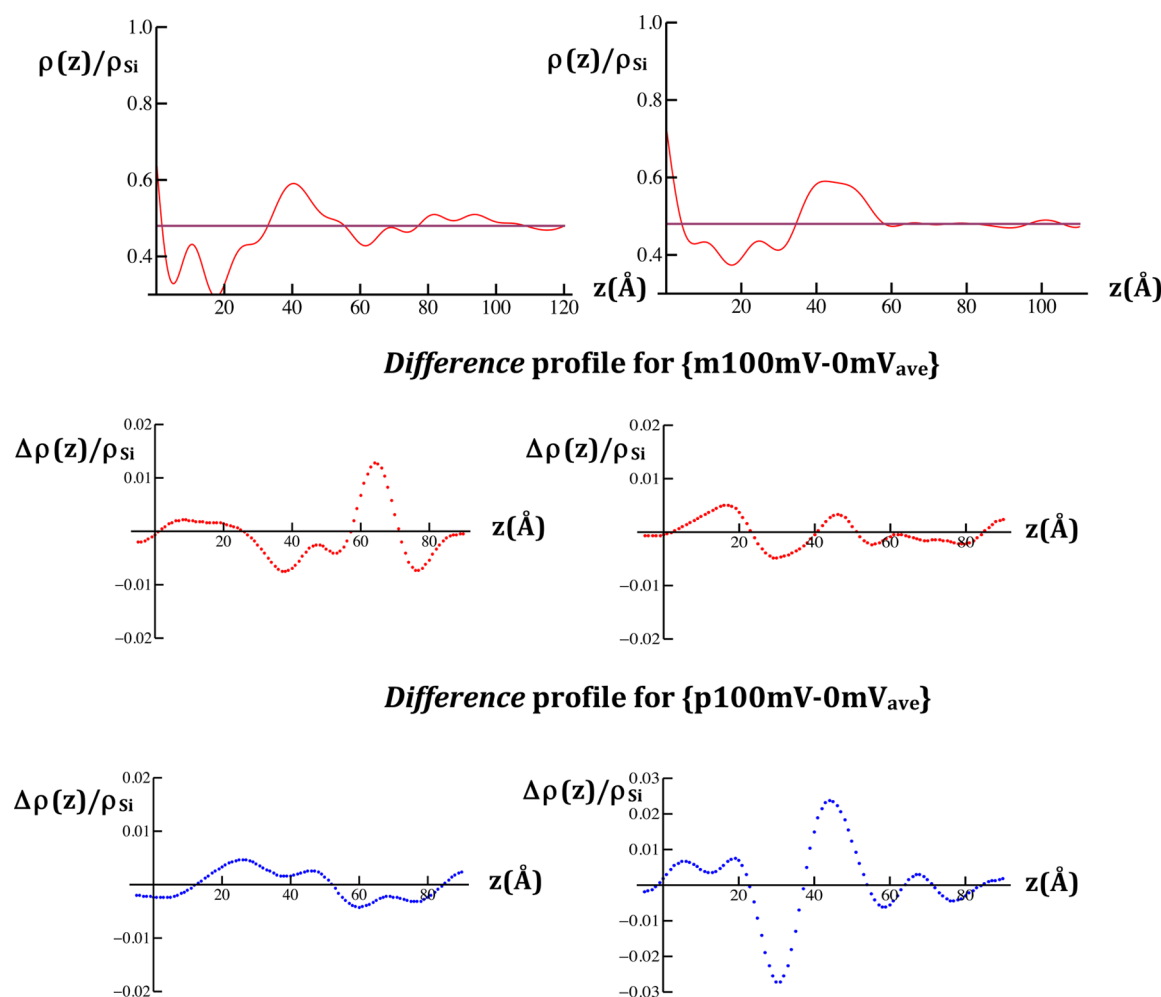
Figure 3. Reduced X-ray scattering-length density (xSLD) profiles, $\rho(z)/\rho_{Si}$, calculated for the VSD:POPC membrane tethered to the surface of a SiGeSi multilayer substrate (upper left) and the OTS:POPC hybrid bilayer tethered to the surface of a SiGeSi multilayer substrate (upper right), each at a transmembrane potential of 0 mV. The profile of the multilayer substrate occurs for $z < 0$ Å (see Figure S2 of the Supporting Information, for example). The respective *difference* reduced xSLD profiles, $\Delta\rho(z)/\rho_{Si}$ for each case are shown in the panels below for the pairs of potentials indicated.

X-ray and Neutron Interferometry Data Analysis. We analyzed the X-ray and neutron interferometry data in the first Born approximation, which employs the Fresnel-normalized specular X-ray/neutron reflectivity, $R(Q_z)/R_F(Q_z)$, where $R(Q_z)$ is the experimental specular reflectivity and $R_F(Q_z)$ is the Fresnel function. The Fresnel-normalized reflectivity is proportional to the modulus square of the Fourier transform $F(Q_z)$ of the gradient of the scattering-length density (SLD) profile $d\rho(z)/dz$, where the profile z-axis is normal to the plane of the interfaces(s) comprising the system of interest.[23] The modulus data, $|F(Q_z)|$, were used in our analysis. The standard errors in these data are expressed in terms of the counting statistics. These errors were propagated through the data reduction procedure, including the footprint correction, the correction for off-specular reflectivity, and division by the Fresnel function for an ideal interface. It is essential to note that this procedure *was precisely the same employing the same parameters*, irrespective of the specimen or the applied potential for each reflectivity technique.

The gradient xSLD or nSLD profile, $[d\rho(z)/dz]_{0 \, mV}$ or $[d\rho_b(z)/dz]_{0 \, mV}$, respectively, for a particular specimen was calculated from its respective modulus data, $|F(Q_z)|$, at 0 mV potential utilizing a constrained refinement method to solve the phase problem, the integral of the gradient profile providing the xSLD or nSLD profile itself, $\rho(z, \, e/Å^3)$ or $\rho_b(z, \, 10^{-6}/ \, Å^2)$, as fully described in prior publications.[17,19] Two key constraints are utilized, namely the SLD profile of the inorganic multilayer substrate determined independently

and the extent of the SLD profile of the multilayer with the adsorbed bio-organic overlayer determined independently from the autocorrelation of its gradient profile $\{d\rho(z)/dz \otimes d\rho(-z)/dz\}$.

We then determined the *difference* between the xSLD or nSLD profile for a particular potential of ±100 mV versus that at 0 mV, $[\Delta\rho(z, \, e/Å^3)]_{\pm100 \, mV}$ or $[\Delta\rho_b(z, \, 10^{-6}/Å^2)]_{\pm100 \, mV}$, by analyzing the *difference* modulus data,[24,25] $\Delta|F(Q_z)| = \{|F_{\pm100 \, mV} \, (Q_z)| - |F_{0 \, mV}(Q_z)|\}$, as fully described in the Supporting Information. The analysis constrained any potential differences within the region of the *difference* SLD profiles occupied by the inorganic multilayer substrate to be negligible, compared to those within the membrane tethered to its surface.

Molecular Dynamics Simulation of a VSD:POPC Membrane as a Function of the Membrane Potential. The dependence of the experimental xSLD and nSLD profiles on the transmembrane potential was compared with those calculated from molecular dynamics simulations of a system of one VSD embedded in an extended symmetric bilayer composed of 232 POPC molecules in a symmetric water environment.[26] In order to make this comparison with the experimental system, only the VSD's nearest-neighbor lipids were utilized in order to reduce the lipid/protein mole ratio to that comparable to the experiments, and the profiles for this truncated membrane were then calculated from the trajectories at the same potentials of 0 and ±100 mV averaged over several microseconds, prior to calculating the *difference* time-averaged xSLD and nSLD

profiles used in the comparison, as fully described in the Supporting Information.

RESULTS

Electrical Properties of the Reconstituted VSD:POPC Membranes and the Hybrid OTS:POPC Bilayers. As described in the Experimental Methods, the electrochemical cells were somewhat different for the X-ray interferometry and neutron interferometry experiments, particularly with regard to the manner by which the electrolyte was contained. For the cell used in the X-ray experiments, the resistance of the silicon oxide surface was typically ~200 KΩ/cm^2 for the Si−Ge−Si multilayer reference structures fabricated on silicon. For the reconstituted VSD:POPC membranes, the resistance typically varied from 200 to 400 KΩ/cm^2 with a capacitance of typically 2−3 μF/cm^2. For the hybrid OTS:POPC bilayer membranes, the resistance typically varied from 250 to 350 KΩ/cm^2 with a capacitance of typically 1−2 μF/cm^2. For the more tightly sealed cell used in the neutron experiments, the resistance of the silicon oxide surface increased to 300−400 KΩ/cm^2 for the Si−Ni−Si multilayer reference structures fabricated on silicon. For the reconstituted VSD:POPC membranes, the resistance increased to 600−700 KΩ/cm^2 with the capacitance decreasing to 1−2 μF/cm^2. For the hybrid bilayer membranes, the resistance increased to 1−2 MΩ/cm^2 and the capacitance decreased to 0.4−0.6 μF/cm^2. Examples of the fit of the equivalent circuit model to the EIS data from the cell used in the neutron experiments for the VSD:POPC membrane, the hybrid OTS:POPC bilayer, and the SAM used to tether the VSD:POPC membrane to the surface of the SiNiSi substrate are shown in Figure S8 of the Supporting Information. In view of these EIS results, we estimate that the potentials across the VSD:POPC membrane are likely to be only 50−70% of the potentials applied to the electrodes for either the X-ray or neutron interferometry experiments, and similarly for the hybrid OTS:POPC bilayer for the X-ray interferometry experiments, reported herein.

Time-Resolved X-ray Interferometry of the Reconstituted VSD:POPC Membranes and the Hybrid OTS:POPC Bilayers. Typical modulus data $|F(Q_z)|$ from a VSD:POPC membrane tethered to the surface of a SiGeSi multilayer substrate, prepared via "directed assembly (DA)",[17] for the first two cycles of variation of the transmembrane potential are shown in Figure 2. The potential dependence of the modulus data was used for subsequent analysis. Since the *difference* in the modulus data between p100 mV or m100 mV ("p"/"m" denote +/−, respectively) and 0 mV were similar using the data for either the first or last 0 mV potential in each cycle, the data for the two 0 mV values were averaged. The *difference* modulus data for {p100mV-0mVave}, {m100mV-0mVave}, and {p100mV-m100mV} are also shown in Figure 3. Such difference modulus data were similar for the first two cycles of the transmembrane potential and are significant because the difference data exceed the standard errors and they depend on the particular pair of potentials utilized. Comparable *difference* modulus data were also obtained from a VSD:POPC membrane, prepared via "self assembly (SA)",[17] for the first two cycles of variation of the transmembrane potential, thereby providing additional support for the reproducibility of these data specimen-to-specimen. By the third and fourth cycles, some evolution of the modulus data became evident, possibly arising from radiation damage; the analyses of these data will therefore not be presented here. A hybrid bilayer membrane,

composed of a chemisorbed layer of OTS with an overlayer of POPC lacking the VSD protein, was employed in this work primarily only *as a control*. Typical modulus data for $F(Q_z)$ from the OTS:POPC hybrid bilayer for the first two cycles of variation of the transmembrane potential are shown in Figure 2. The *difference* modulus data for {p100mV-0mVave} and {m100mV-0mVave} are also shown in Figure 2. These difference modulus data were also similar for the first two cycles of the transmembrane potential and are significant because the difference data exceed the standard errors and they depend on the particular pair of potentials utilized. The difference modulus data for the OTS:POPC hybrid bilayer differ dramatically from those for the VSD:POPC membrane, thereby providing an important control in momentum transfer space.

The xSLD profiles and their dependence on the applied potentials, as expressed in *difference* xSLD profiles, were calculated from the modulus and *difference* modulus data, respectively, as described in the Experimental Methods. A typical xSLD profile for the VSD:POPC membrane at 0 mV is shown in Figure 3, along with the *difference* xSLD profiles for {p100mV-0mVave} and {m100mV-0mVave}. By comparison with Figure S1 in the Supporting Information, the VSD:POPC membrane for these specimens is about 70 Å in total thickness and occurs within 25 Å < z < 95 Å of the xSLD profile. The *difference* profiles exhibit substantial changes throughout the extent of the membrane profile and are distinctly different depending on the particular potentials utilized. In particular, for the potential pair {m100mV-0mVave}, the major changes involve a larger increase in electron density (xSLD) over the region 55 Å < z < 70 Å and corresponding lesser decreases in electron density over the two adjacent regions 30 Å < z < 55 Å and 70 Å < z < 85 Å of the membrane profile. For the potential pair {p100mV-0mVave}, the major changes involve an increase in electron density (xSLD) over the region 15 Å < z < 50 Å and a corresponding decrease in electron density of comparable magnitude over the adjacent region 50 Å < z < 85 Å of the membrane profile.

A typical xSLD profile for the OTS:POPC hybrid bilayer lacking the VSD protein at 0 mV along with the *difference* xSLD profiles for {p100mV-0mVave} and {m100mV-0mVave} are also shown in Figure 3. The OTS:POPC hybrid bilayer for these specimens occurs within 0 Å < z < 50 Å of the xSLD profile. The hydrocarbon core of the bilayer occurs within 5 Å < z < 35 Å and the POPC polar headgroups within 35 Å < z < 55 Å. We note that the layer of POPC polar headgroups is somewhat thicker than expected by ~5 Å, given the spatial resolution of these profiles (~13 Å), which may arise from the surface roughness of the SiGeSi multilayer substrates. The *difference* profiles exhibit substantial changes throughout the extent of bilayer profile, and they are distinctly different depending on the particular potentials utilized. In particular, for the potential pair {m100mV-0mVave}, the major changes involve increases in electron density (xSLD) over the regions 10 Å < z < 25 Å and 40 Å < z < 50 Å and a corresponding decrease in electron density of comparable magnitude over the intervening region 25 Å < z < 40 Å of the bilayer profile. For the potential pair {p100mV-0mVave}, the major changes involve a large increase in electron density (xSLD) over the region 35 Å < z < 55 Å and a corresponding decrease in electron density of comparable magnitude over the adjacent region 25 Å < z < 35 Å of the bilayer profile. Importantly, these changes are very different from those for the VSD:POPC
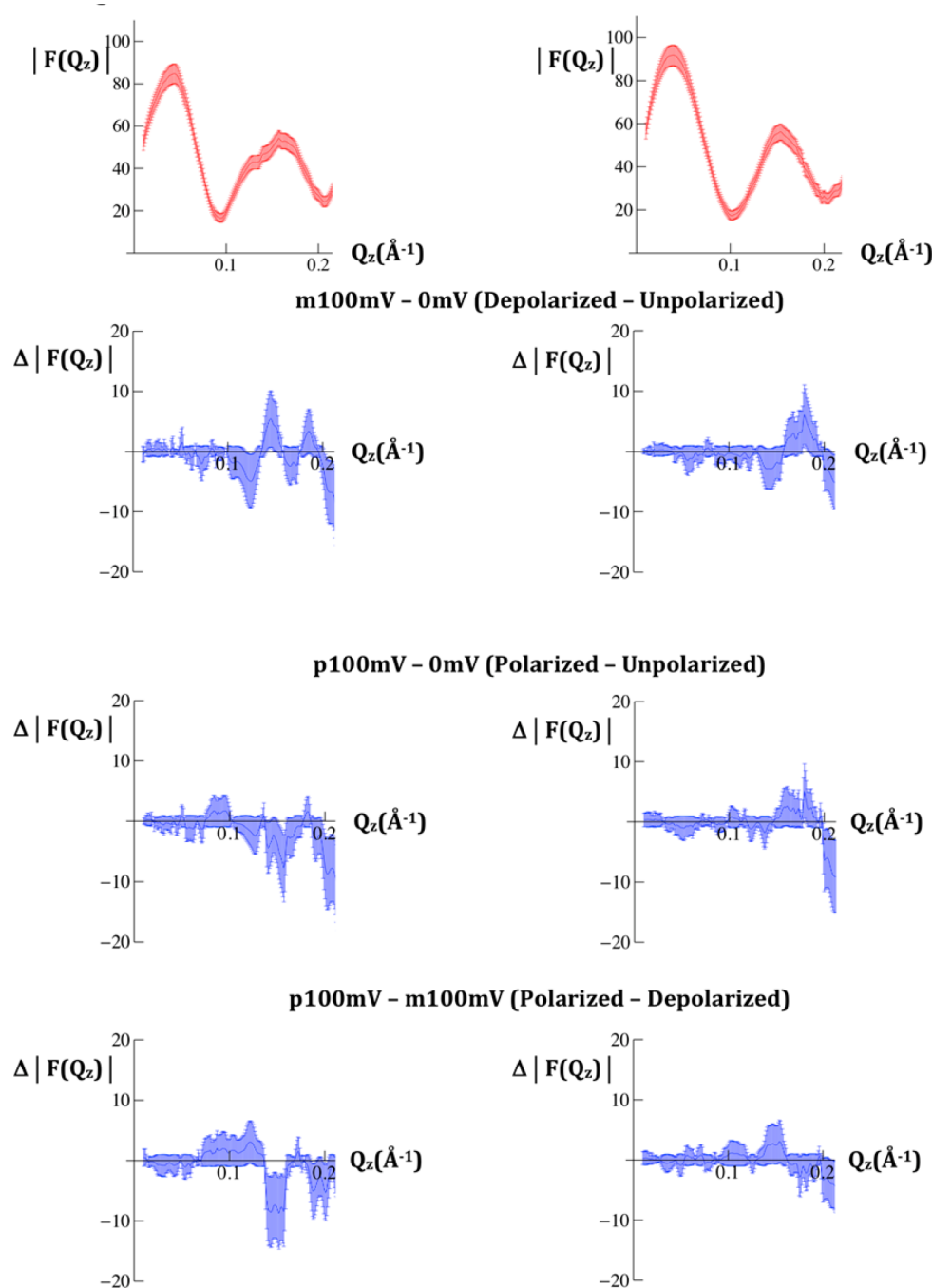
Figure 4. Modulus |F(Q_z)| data calculated from the specular neutron reflectivity $R(Q_z)/R_F(Q_z)$, where $|F(Q_z)|^2 = R(Q_z)/R_F(Q_z)$, for the VSD:POPC membrane tethered to the surface of a SiNiSi multilayer substrate (upper left) and for the SAM chemisorbed onto the surface of a SiNiSi multilayer substrate (upper right), each at a transmembrane potential of 0 mV. The respective *difference* modulus data $\Delta|F(Q_z)|$ for each case are shown in the panels below for the pairs of potentials indicated. The standard errors in the data are indicated for each case.

membrane described above, the comparison facilitated by their juxtaposition in Figure 3, thereby providing an essential control in real space.

While the standard errors are readily apparent in the modulus data, they are not so evident in the Fourier analysis of these data. However, the control experiments utilized herein provide an important measure of these errors propagated through the analysis. In the X-ray case, the low amplitude, short wavelength fluctuations arising from transform truncation in the reduced xSLD profile for the OTS:POPC hybrid bilayer within the region 60 Å < z < 120 Å, occupied only by the

aqueous electrolyte where the profile should be flat, indicate that the propagated errors remain below the 5% level (with reference to Figure 3; right side, top panel). The propagated errors are thereby seen to rise to the 10% level within the same region of the *difference* xSLD profiles (with reference to Figure 3; right side, middle and lower panels).

Time-Resolved Neutron Interferometry of the Reconstituted VSD:POPC Membranes and the Hybrid OTS:POPC Bilayers. Unlike the case with X-rays, neutrons produce little radiation damage. The modulus data for $F(Q_z)$ from the Fresnel-normalized neutron reflectivity data from a
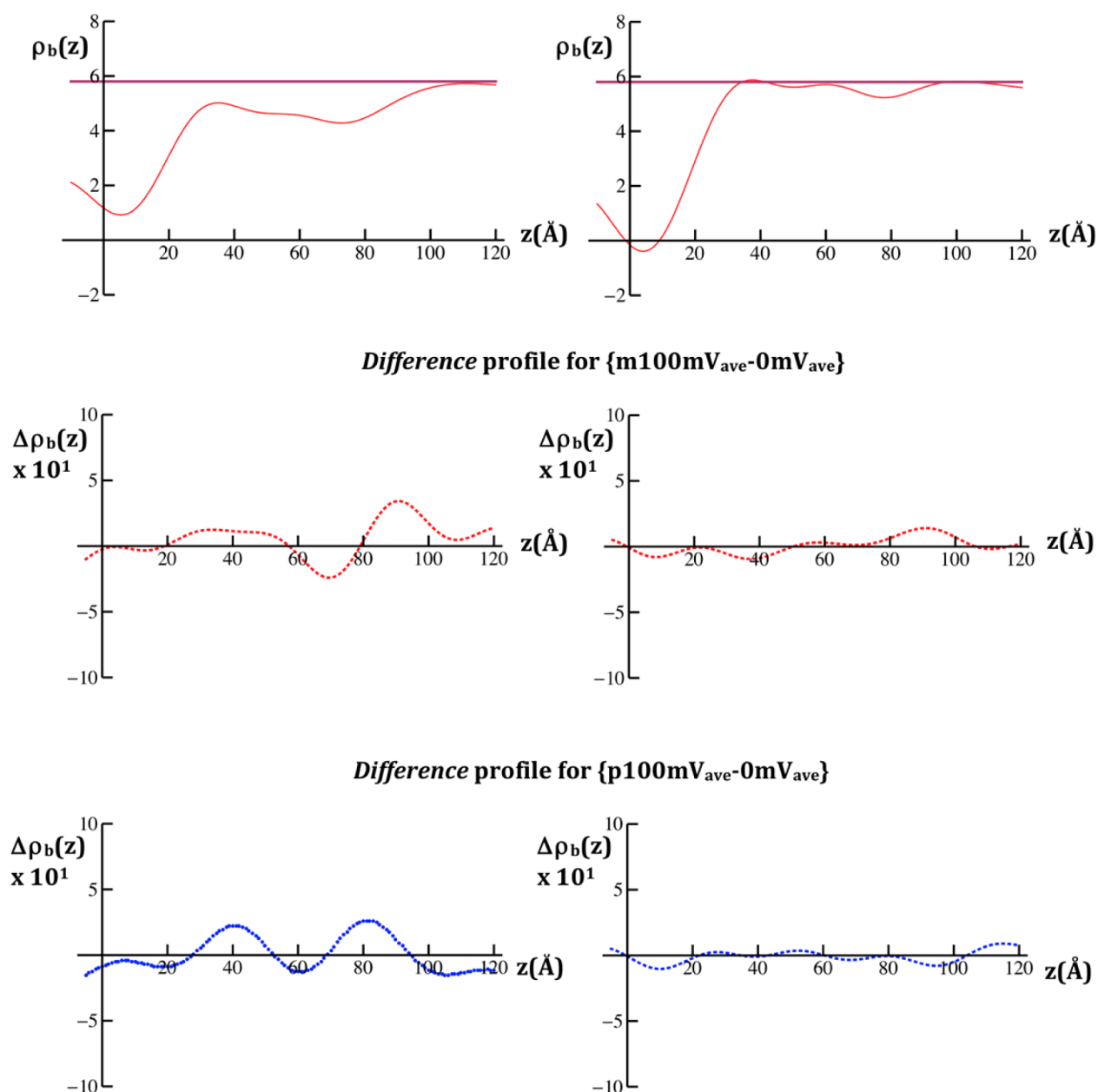
Figure 5. Neutron scattering-length density (nSLD) profiles, $\rho_b(z)$, calculated for the VSD:POPC membrane tethered to the surface of a SiNiSi multilayer substrate (upper left) and for the SAM chemisorbed onto the surface of a SiNiSi multilayer substrate (upper right), each at a transmembrane potential of 0 mV. The aqueous buffered KCl electrolyte was in 90% D_2O:10% H_2O. The respective *difference* nSLD profiles, $\Delta\rho_b(z)$, for each case are shown in the panels below for the pairs of potentials indicated. The nSLD profiles are in units of $10^{-6}/$ Å^2.

VSD:POPC membrane, prepared via "self assembly (SA)",[17] is shown in Figure 4. In this case, the control was composed of only the chemisorbed organic chain molecules, or SAM, used to tether the VSD protein to the inorganic substrate surface, thus lacking the VSD protein. The modulus data for this control SAM are also shown in Figure 4. The *difference* modulus data for {p100mV-0mVave}, {m100mV-0mVave}, and {p100mV-m100mV} are shown in Figure 4 for both the membrane and the SAM. The errors for both the membrane and SAM are larger than those for the X-ray case. Nevertheless, the difference data remain significant as they barely exceed the standard errors, they depend on the particular pair of potentials utilized, and they differ between the VSD:POPC membrane and the control SAM lacking VSD protein.

The nSLD profiles and their dependence on the applied potentials, as expressed in *difference* nSLD profiles, were calculated from the modulus and *difference* modulus data, respectively, as described in the Experimental Methods. In Figure 5, we compare the nSLD profile at 0 mV and the *difference* nSLD profiles for {p100mV-0mVave} and {m100mV-0mVave} for the VSD:POPC membrane with those from the SAM. By comparison with Figure S1 in the Supporting Information, the VSD:POPC membrane for these specimens occurs within 25 Å < z < 95 Å of the nSLD profile. The *difference* profiles exhibit substantial changes throughout the extent of VSD:POPC membrane profile and are distinctly different depending on the particular potentials utilized. In particular, for the potential pair {m100mV-0mVave}, the major changes involve an increase in nSLD over the region 80 Å < z <
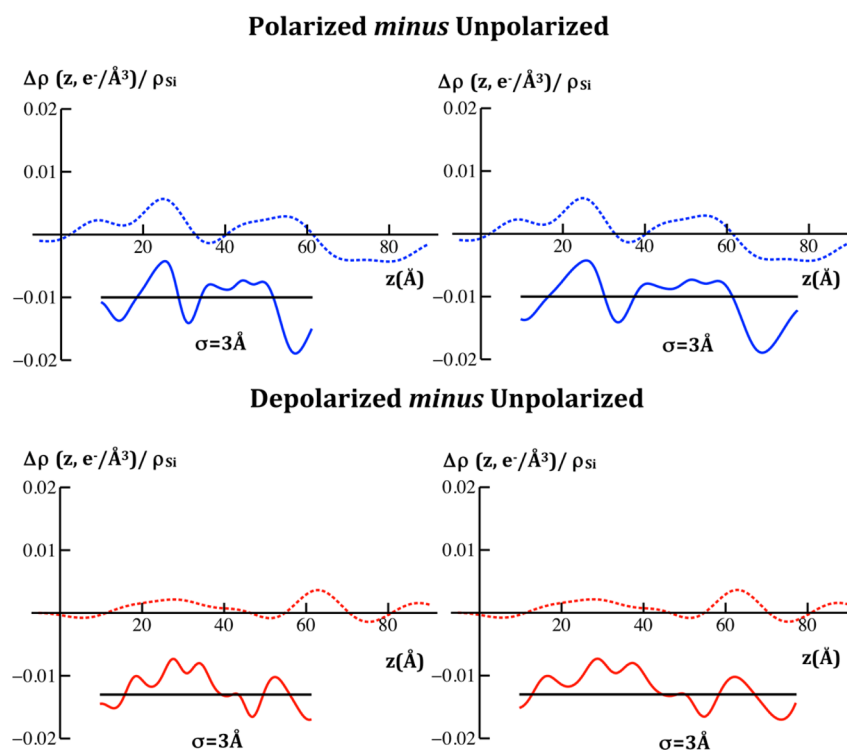
Figure 6. Left side: comparison of the *difference* xSLD profiles determined from the X-ray interferometry experiments for VSD:POPC membrane tethered to the surface of an inorganic multilayer substrate (dotted) from the first cycle of the series of potentials applied, with those calculated from molecular dynamics simulations for an untethered VSD:POPC membrane (solid) for the two pairs of potentials indicated, each membrane fully hydrated. Right side: the same comparison, but with the abscissa scale for the *difference* profiles calculated from the simulation expanded by 25%. The time-averaged profiles calculated from the simulations have been smoothed via convolution with a Gaussian whose 1/e width was 2σ.

100 Å and corresponding decrease in nSLD over the adjacent region 55 Å $< z <$ 80 Å of the membrane profile. For the potential pair {p100mV-0mVave}, the major changes involve a comparable increase in nSLD over the two regions 30 Å $< z <$ 50 Å and 70 Å $< z <$ 90 Å, with smaller decreases in nSLD for the region $z <$ 30 Å and the intervening region 50 Å $< z <$ 70 Å of the membrane profile. The corresponding *difference* profiles for the SAM are essentially featureless, again providing an essential control in real space.

Again, while the standard errors are readily apparent in the modulus data, they are not so evident in the Fourier analysis of these data. The control experiments utilized provide an important measure of these errors propagated through the analysis. In the neutron case, the low amplitude, short wavelength fluctuations arising from transform truncation in the reduced nSLD profile for the SAM within the region 40 Å $< z <$ 120 Å, occupied only by the aqueous electrolyte where the profile should be flat, indicate that the propagated errors are larger but remain below the 10% level (with reference to Figure 5; right side, top panel). The propagated errors are thereby seen to rise to the 20% level within the same region of the *difference* nSLD profiles (with reference to Figure 5; right side, middle and lower panels).

■ DISCUSSION

As described in the Introduction, the structure of the reconstituted VSD:POPC membranes central to these studies has been extensively characterized by both X-ray and neutron interferometry in prior work.[17,19] Their electrical properties within the electrochemical cells utilized in this work have been found sufficient to support transmembrane electric potentials,

although these are only 50−70% of the potentials applied to the electrodes due to the presence of a silicon oxide layer on the surface of the inorganic substrates to which the membranes are tethered. The structure of the OTS:POPC bilayer, utilized only as a control in these studies, has also been characterized by X-ray interferometry. Its electrical properties within the electrochemical cells utilized in this work have been found sufficient to support transbilayer electric potentials, although again these are only 50−70% of the potentials applied to the electrodes.

The results from both the time-resolved X-ray and neutron interferometry experiments described demonstrate directly that significant changes occur throughout the profile structure of the VSD:POPC membrane upon application of a transmembrane electric potential, and the changes depend on the sign of the applied potential with respect to zero potential. With reference to the resting potential of the natural membrane,[1,2] for the vectorial orientation of the VSD within the membrane in our electrochemical cells, {p100mV-0mV} would refer to a "polarizing" potential difference while {m100mV-0mV} would refer to a "depolarizing" potential difference. Such potential-dependent changes are either completely different for the OTS:POPC hybrid bilayer membrane or essentially absent for the SAM, both serving as important controls lacking the VSD protein. Since the physical origin of the atomic scattering factors for X-rays and neutrons is entirely different, the latter being much more sensitive to the distribution of exchangeable hydrogen including water, we have therefore verified the existence of potential-dependent changes within the profile structure of the VSD:POPC membrane by two independent scattering methods. In addition, the difference SLD profiles for the depolarizing potential pair {m100mV-0mV} convincingly

demonstrate that a potential of 0 mV does not produce the depolarized state of the VSD, as has been commonly assumed [e.g., refs 3−6, etc.]. It is important to note that these new experimental results stand on their own, in the sense that any modeling of their structural significance at the 3-D atomic-level must account for the changes in the profile structure described.

Prior to addressing the structural significance of the observed potential-dependent changes in the SLD profiles, it is important to reiterate that the changes described were both reproducible and reversible. Reproducibility for both the X-ray and neutron experiments is described in some detail in the Supporting Information. The "inactivation" associated with the complete KvAP channel (from which the VSD was derived) in electrophysiological experiments,[27] arising from multiple cycles of depolarization and repolarization of the membrane potential on a time scale of 100−200 ms per potential, could have undermined these experiments. In the X-ray case, it was not necessary to average over multiple cycles, and the experimental modulus data for the two 0 mV potentials employed within each of the four cycles investigated superimposed to within the noise level, demonstrating reversibility despite the longer time scale of 5−20 s per potential. Furthermore, the potential-dependent changes in the xSLD profiles were similar for the first and second cycles, in terms of the positions and amplitudes of their major features as evident from a comparison of Figures 3 and 6, although they do differ in detail. Neither would have occurred with any substantial level of inactivation comparable to that for the complete KvAP channel, for which the entire ensemble becomes inactivated after only three cycles.[27] For the neutron case, averaging over many cycles was required to achieve a satisfactory noise level in the modulus data for each value of the potential. Again, if inactivation on a time scale of 20 s, comparable to that for the complete KvAP channel, had been a major factor cycle-to-cycle, potential-dependent changes in the modulus data would have vanished with averaging over many cycles. Thus, the inactivation associated with the complete channel does not appear to play any significant role in these studies of the isolated VSD protein.

The difference in the physical origin of the atomic scattering factors for X-rays and neutrons noted above makes it difficult to compare xSLD and nSLD profiles, and their respective potential-dependent difference profiles employed in this work, in the absence of a detailed atomic-level model for the VSD:POPC membrane. Furthermore, given the complexity of the membrane, and the fact that the profile structure is a 1-D projection of the 3-D structure, the observed changes in the profile structure of the VSD:POPC membrane, in terms of its xSLD and nSLD profiles, have no simple interpretation. However, both the VSD itself[28] and in a full-length Kv-channel[29] within fully hydrated POPC membranes have been extensively investigated recently via molecular dynamics simulations *as a function of* the applied transmembrane electric potential. Such simulations of only a single VSD or full-length Kv-channel protein within the hydrated bilayer membrane require very long trajectories (10 and 100 μs time scale, respectively) as made possible by Anton, a special-purpose supercomputer for molecular dynamics simulations.[30] Since these simulations contain the full 3-D atomic-level structure of the complex membrane system, it is straightforward to calculate its projected profile structure, time-averaged over a selected segment near the end of the trajectory over which the structure exhibits stability.

In Figure 6, we compare the *difference* xSLD profile structures from the experiments reported here for the first cycle in the variation of the transmembrane potential with those calculated from the simulations of the VSD within a fully hydrated POPC membrane[26,28] for both the polarizing and depolarizing cases as defined above. It is essential to note here that although the simulations were for an isolated VSD, they were set up based on indirect experimental data on the complete KvAP channel,[3,10] thereby biasing the results toward those for the VSD within the complete channel. The agreement from this comparison is only qualitative because although the difference profiles exhibit very similar shapes (using "similar" in the geometric sense), the membrane profile from the simulations appears ∼20−25% thinner than those for the tethered membrane in the experiments.[17,19] For the purpose of demonstrating this geometric similarity, a 25% expansion of the abscissa scale for the simulation can readily be seen to improve the agreement between the experiments and the simulation, as also shown in Figure 6. This agreement between the experiment and the simulation is slightly better for the first cycle in the variation of the potential, as shown, than for the second cycle (not shown). In Figure 7, we compare the *difference* nSLD profile structures from the experiments reported here, in which the interferometric data for each
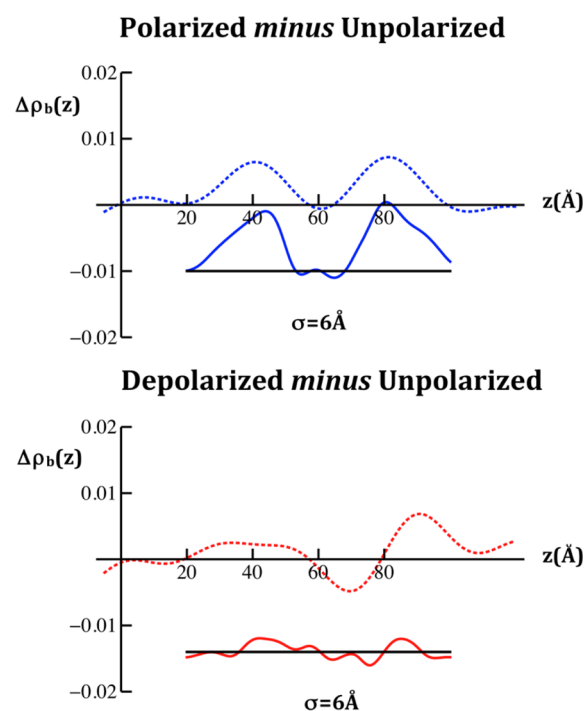

Figure 7. Comparison of the *difference* nSLD profiles determined from the neutron interferometry experiments for VSD:POPC membrane tethered to the surface of an inorganic multilayer substrate (dotted) with those calculated from molecular dynamics simulations for an untethered VSD:POPC membrane (solid) for the two pairs of potentials indicated, each membrane fully hydrated. As with the comparison of the *difference* xSLD profiles shown in Figure 6, we show here only the case where the abscissa scale for the *difference* profiles calculated from the simulation have been expanded by 25%. The time-averaged profiles calculated from the simulations have been smoothed via convolution with a Gaussian whose $1/e$ width was 2σ, the larger value used here to allow for the lower spatial resolution of the nSLD profiles. We note that the nSLD profiles shown here are in units of $10^{-4}/\text{Å}^2$.
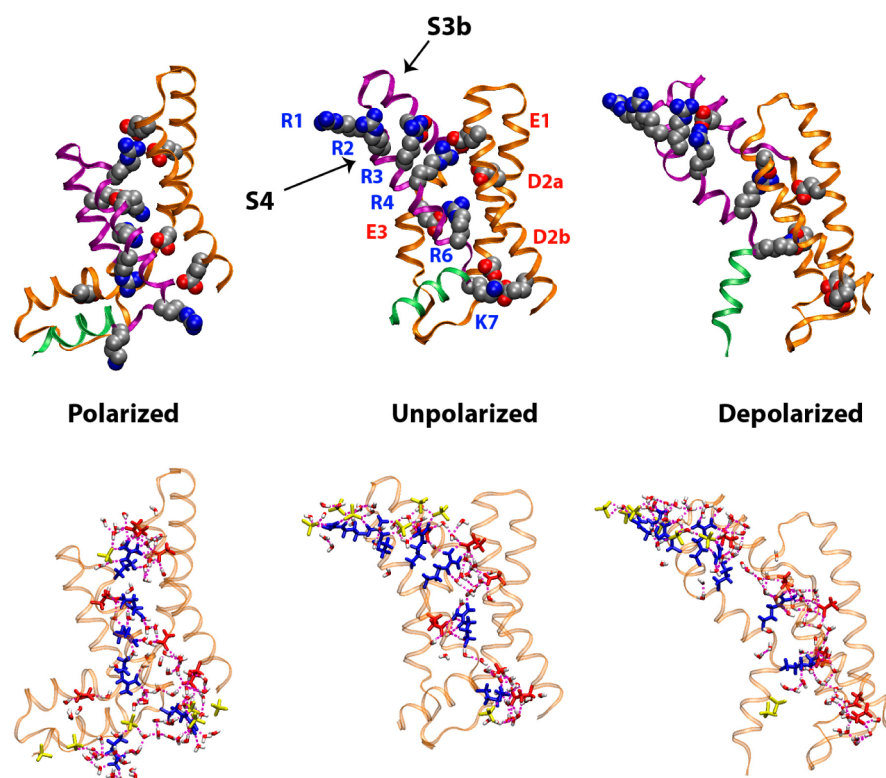
Figure 8. VSD configurations from microsecond time scale atomistic MD simulations. Top row: the VSD backbone is shown in ribbon representation with the S1−S3a segments colored orange, the S3b−S4 helix-turn-helix in purple, and the S4−S5 linker in green. Conserved charged side chains (shown as filled spheres) are colored by atom type (carbon, silver; oxygen, red; nitrogen, blue). Upon a change in applied membrane potential, the motion of the highly conserved basic side chains on (R1 through K7) on the S4 helix induces conformational changes in the S3b−S4 helical hairpin. As the basic side chains move within the membrane electric field, they exchange salt-bridge interactions with acidic side chains in conserved positions (E1, D2a, D2b, and E3) as well as two additional acidic side chains in S3b and S1 (unlabeled). Bottom row: the solvation of the VSD by the membrane environment is represented as a H bond network between the VSD basic and acidic side chains (blue and red, respectively), lipid phosphate groups (yellow), and waters (colored by atom type).

value of the potential was an average over many cycles in the variation of the transmembrane potential, with those calculated from the simulations for the VSD within a fully hydrated POPC membrane[26,28] for both the polarizing and depolarizing cases as defined above. Here, we show only the case for the 25% expansion of the abscissa scale. Like the X-ray case, the experimental *difference* nSLD profiles have very similar geometric shapes compared to their counterparts from these simulations.

There may be an explanation for the larger extent of the VSD:POPC membrane profile in our experiments arising from differences in the X-ray crystal[6] and NMR solution[7] structures of the isolated, detergent-solubilized VSD compared to that within the X-ray crystal structure of the complete Kv channel[3] utilized in the simulations. First, the VSD protein construct in the experiments includes 18 additional residues on the N-terminus that were not explicitly modeled in the simulations, since it only appears in the NMR solution structure of the isolated VSD. Ten residues in this sequence form an α-helix (designated as the S0 helix) that, while not expected to change configuration under an applied potential, would occur on the proximal side of the membrane (with respect to the substrate surface). It could increase the overall membrane thickness by as much as 15 Å, were its orientation approximately parallel to the axis of the transmembrane 4-helix bundle structure formed by helices S1−S4 of the VSD, as in the NMR structure,[7] and thereby approximately perpendicular to the membrane surface.

Second, in the simulations, the 12-residue S4−S5 linker helix was aligned nearly parallel to the membrane surface as within the X-ray structure of the complete Kv channel,[3] unlike that for the isolated VSD[6,7] in these experiments where the linker helix is an linear extension of the S4 transmembrane helix, thereby extending the length of the S4 helix in the transmembrane direction by as much as 18 Å, again depending on its precise orientation approximately perpendicular to the membrane surface. Thus, favorable orientations of the S0 helix and of the S4−S5 linker helix on the proximal side of the membrane approximately perpendicular to the membrane surface, associated with the very low lipid content of the membrane of only ~24 POPC nearest-neighbor molecules per VSD[17,19] in these experiments, would be sufficient to explain the increase in the profile extent of the membrane dominated by the VSD protein, namely from ~55 Å in the simulations to ~70 Å, or by ~25%. Furthermore, potential-dependent changes in the profile would also be expected to occur over this increased extent given the likely origin of the conformational changes expected in the VSD that involve translation of the S4 helix in the transmembrane direction, as described below, that would likely include the translation of its linear extension through the S4−S5 linker helix for the isolated VSD.

The qualitative level of agreement between experiments and simulations, as shown in Figures 6 and 7, suggests that the voltage-dependent changes observed in the SLD profiles arise from conformational changes in the isolated VSD that include

an effective displacement of the helical hairpin formed by the S4 helix and the C-terminal half of the S3 helix (termed S3b), as depicted in Figure 8, similar to those measured indirectly within the complete Kv channel.[10,31] The basic side chains in S4 contribute most of the charge that give rise to the gating currents in electrophysiology experiments.[1,32] The simulations used here predict a substantial translational motion of the S4 helix along the transmembrane direction of 10−12 Å between the depolarized and the polarized states. The indirect experiments on the complete Kv channel suggest that the magnitude of this displacement may be slightly larger of 12−15 Å (see Figure 2 in ref 26 for a direct comparison). Importantly, these particular conformational changes must result in the propagation of changes over the entire ~60 Å extent of the profile structure of the isolated VSD, as evident from the qualitative level of agreement between the experiments and the simulations. A key structural feature of the membrane-embedded VSD predicted by simulations and confirmed by neutron interferometry[19] is that the interior of the VSD is hydrated along the entire length of its profile. Our simulations suggest that measured gating charge displacements are the result of water-catalyzed rearrangements of salt bridges between the S4 basic side chains and the set of conserved acidic side chains on the S1−S3 helical segments in the hydrated interior of the VSD (Figure 8), an observation that is consistent with more extensive simulations of the Kv full-length channel performed in the absence of any experimental restraints.[29] These specific structural and mechanistic models gain definitive support from the direct measurements of potential-dependent structural changes within the isolated VSD protein reported here.

Nevertheless, in order to obtain a more quantitative level of agreement with the experiments, the simulations would need to be modified to better represent the application of trans-membrane electric potentials to a tethered VSD:POPC membrane more closely approximating that of the experiments, specifically with regard to the asymmetric profile structure of the POPC bilayer and the elongated profile extension of the isolated VSD protein within the membrane, as well as the partial hydration on the proximal side of the membrane in contrast to the full hydration of its distal side. Such simulations are a substantial investigation on their own beyond the scope of this work. In addition, we anticipate that the experimental structural results will be further refined in the future to define the potential-dependent positions of the key elements of helical secondary structure within the isolated VSD, employing site-directed labeling with methyl-Hg for time-resolved resonance X-ray interferometry and site-specific deuterium labeling (enabled by protein semisynthesis[33]) for time-resolved neutron interferometry.

Lastly, we note that the time-resolved X-ray interferometry approach can be also applied to the complete KvAP channel,[17] despite its inactivation associated with multiple cycles of depolarization and repolarization,[27] because satisfactory stand-ard errors can be achieved within a single cycle. This will allow a more definitive comparison of the conformational changes within the VSD's profile structure associated with voltage gating for the isolated VSD with those for the VSD within the complete Kv channel, due to the distinct advantage of utilizing the same direct method on each of the two proteins under otherwise identical experimental conditions.

■ CONCLUSION

In contrast with prior studies, this work describes the measurement of changes in the structure of the isolated VSD protein, vectorially oriented within a reconstituted phospholipid bilayer membrane, as a function of the transmembrane electric potential using two direct and independent scattering techniques. Time-resolved X-ray interferometry and time-resolved neutron interferometry have been employed to provide the dependence of their respective scattering-length density (xSLD and nSLD) profiles at three values of the potential spanning the physiological range. The results convincingly demonstrate that a potential of 0 mV does not actually produce the depolarized state of the VSD, as has been commonly assumed. The changes in the experimental xSLD and nSLD profiles for both polarizing and depolarizing potentials with respect to zero potential extend over the entire ~60 Å length of the profile structure of the isolated VSD. These changes are in qualitative agreement with molecular dynamics simulations of a related membrane system, thus suggesting a possible origin of these changes in terms of the isolated VSD's atomic-level 3-D structure.

■ ASSOCIATED CONTENT

ⓢ Supporting Information

Experimental details; Figures S1−S8. This material is available free of charge via the Internet at http://pubs.acs.org.

■ AUTHOR INFORMATION

Corresponding Author

*E-mail jkblasie@sas.upenn.edu (J.K.B.).

Notes

The authors declare no competing financial interest.

■ ACKNOWLEDGMENTS

■ REFERENCES

(1) Bezanilla, F. The Voltage Sensor in Voltage-Dependent Ion Channels. *Physiol. Rev.* **2000**, *80* (2), 555−592.

(2) Sigworth, F. J. Structural Biology: Life's Transistors. *Nature* **2003**, *423* (6935), 21−22.

(3) Lee, S.-Y.; Lee, A.; Chen, J.; MacKinnon, R. Structure of the KvAP Voltage-dependent K⁺ Channel and Its Dependence on the Lipid Membrane. *Proc. Natl. Acad. Sci. U. S. A.* **2005**, *102*, 15441−15446.

(4) Long, S. B.; Tao, X.; Campbell, E. B.; MacKinnon, R. Atomic Structure of a Voltage-Dependent K⁺ Channel in a Lipid Membrane-like Environment. *Nature* **2007**, *450*, 376−383.

(5) Payandeh, J.; Scheuer, T.; Zheng, N.; Catterall, W. A. The Crystal Structure of a Voltage-Gated Sodium Channel. *Nature* **2011**, *475*, 353−358.

(6) Jiang, Y.; Lee, A.; Chen, J.; Ruta, V.; Cadene, M.; Chait, B. T.; MacKinnon, R. X-ray Crystal Structure of a Voltage-Dependent K⁺ Channel. *Nature* **2003**, *423*, 33−41.

(7) Butterwick, J. A.; MacKinnon, R. Solution Structure and Phospholipid Interactions of the Isolated Voltage-Sensor Domain from KvAP. *J. Mol. Biol.* **2010**, *403*, 591−606.

(8) Cha, A.; Snyder, G. E.; Selvin, P. R.; Bezanilla, F. Atomic Scale Movement of the Voltage-Sensing Region in a Potassium Channel Measured by Spectroscopy. *Nature* **1999**, *402*, 809−813.

(9) Pathak, M. M.; Yarov-Yarovoy, V.; Agarwal, G.; Roux, B.; Barth, P.; Kohout, S.; Tombola, F.; Isacoff, E. Y. Closing in on the Resting State of the Shaker K(+) Channel. *Neuron* **2007**, *56* (1), 124−140.

(10) Ruta, V.; Chen, J.; MacKinnon, R. Calibrated Measurement of Gating-Charge Arginine Displacement in the KvAP Voltage-Dependent K⁺ Channel. *Cell* **2005**, *123*, 463−475.

(11) Larsson, H. P.; Baker, O. S.; Dhillon, D. S.; Isacoff, E. Y. Transmembrane Movement of the Shaker K⁺ Channel S4. *Neuron* **1996**, *16* (2), 387−397.

(12) Lu, Z.; Klem, A. M.; Ramu, Y. Ion Conduction Pore is Conserved Among Potassium Channels. *Nature* **2001**, *413*, 809−813.

(13) Capasso, M.; DeCoursey, T. E.; Dyer, M. J. S. pH Regulation and Beyond: Unanticipated Functions for the Voltage-Gated Proton Channel HVCN1. *Trends Cell Biol.* **2010**, *21* (1), 20−28.

(14) Halaszovich, C.; Schreiber, D. N.; Oliver, D. Ci-VSP is a Depolarization-Activated Phosphatidylinositol-4,5-biphosphate and Phosphatidylinositol-3,4,5-triphosphate 5′-Phosphatase. *J. Biol. Chem.* **2009**, *284* (4), 2106−2113.

(15) Takeshita, K.; Sakata, S.; Yamashita, E.; Fujiwara, Y.; Kawanabe, A.; Kurokawa, T.; Okochi, Y.; Matsuda, M.; Narita, H.; Okamura, Y.; Nakagawa, A. X-ray Crystal Structure of Voltage-Gated Proton Channel. *Nat. Struct. Mol. Biol.* **2014**, DOI:10.1038/nsmb.2783.

(16) Li, Q.; Wanderling, S.; Paduch, M.; Medovoy, D.; Singharoy, A.; McGreevy, R.; Villaba-Galea, C. A.; Hulse, R. E.; Roux, B.; Schulten, K.; Kossiakoff, A.; Perozo, E. Structural Mechanism of Voltage-Dependent Gating in an Isolated Voltage-Sensing Domain. *Nat. Struct. Mol. Biol.* **2014**, DOI: 10.1038/nsmb.2768.

(17) Gupta, S.; Liu, J.; Strzalka, J.; Blasie, J. K. Profile Structures of the Voltage-Sensor Domain and the Voltage-Gated K⁺-channel Vectorially-Oriented in a Single Phospholipid Bilayer Membrane at the Solid-Vapor and Solid-Liquid Interfaces *via* X-ray Interferometry. *Phys. Rev. E* **2011**, *84* (3), 031911−1−15.

(18) Krishnan, V.; Strzalka, J.; Liu, J.; Liu, C.; Kuzmenko, I.; Gog, T.; Blasie, J. K. Interferometric Enhancement of X-ray Reflectivity from Unperturbed Langmuir Monolayers of Amphiphiles at the Liquid-Gas Interface. *Phys. Rev. E* **2010**, *81*, 021604−1−10.

(19) Gupta, S.; Dura, J.; Freites, A.; Tobias, D.; Blasie, J. K. Structural Characterization of the Voltage Sensor Domain and Voltage-Gated K⁺-Channel Proteins Vectorially-Oriented within a Single Bilayer Membrane at the Solid/Vapor and Solid/Liquid Interfaces *via* Neutron Interferometry. *Langmuir* **2012**, *28* (28), 10504−10520.

(20) Cornell, B. A.; Braach-Maksvytis, V. L. B.; King, L. B.; Osman, P. D. J.; Raguse, B.; Wieczorek, L.; Pace, R. J. *Nature* **1997**, *387*, 580.

(21) Purrucker, O.; Hillebrandt, H.; Adlkoffer, K.; Tanaka, M. Deposition of Highly Resistive Lipid Bilayer on Silicon-Silicon Dioxide Electrode and Incorporation of Gramicidin Studied by AC Impedance Spectroscopy. *Electrochim. Acta* **2001**, *47*, 791−798.

(22) Tronin, A.; Chen, C.-H.; Gupta, S.; Worcester, D.; Lauter, V.; Strzalka, J.; Kuzmenko, I.; Blasie, J. K. Structural Changes in Single Membranes in Response to an Applied Transmembrane Electric Potential Revealed by Time-Resolved Neutron/X-ray Interferometry. *Chem. Phys.* **2013**, *422*, 283−289.

(23) Blasie, J. K.; Strzalka, J.; Zheng, S. Solution to the Phase Problem for Specular X-ray & Neutron Reflectivity from Thin Films on Liquid Surfaces. *Phys. Rev. B* **2003**, *67*, 224201−1−224201−8.

(24) Ramasesahn, S. The Use of Anomalous Scattering in Crystal Structure Analysis. In *Advanced Methods in Crystallography*, 3rd ed.; Ramachandran, G. N., Ed.; Academic Press: New York, 1964.

(25) Asturias, F. J.; Blasie, J. K. Location of the High-Affinity Metal Binding Sites in the Profile Structure of the Ca²⁺-ATPase of the Sarcoplasmic Reticulum by Resonance X-ray Diffraction. *Biophys. J.* **1991**, *59*, 488−502.

(26) Schow, E. V.; Freites, J. A.; Gogna, K.; White, S. H.; Tobias, D. J. Down-State Model of the Voltage-Sensing Domain of a Potassium Channel. *Biophys. J.* **2010**, *98*, 2857−2866.

(27) Schmidt, D.; Cross, S. R.; MacKinnon, R. A Gating Model for the Archeal Voltage-Dependent K⁺ Channel KvAP in DPhPC and POPE:POPG Decane Lipid Bilayers. *J. Mol. Biol.* **2009**, *390* (5), 902−912.

(28) Freites, J. A.; Schow, E. V.; White, S. H.; Tobias, D. J. Microscopic Origin of Gating Current Fluctuations in a Potassium Channel Voltage Sensor. *Biophys. J.* **2012**, *102*, L44−L46.

(29) Jensen, M. Ø.; Jogini, V.; Borhani, D. W.; Leffler, A. E.; Dror, R. O.; Shaw, D. E. Mechanism of Voltage Gating in Potassium Channels. *Science* **2012**, *336*, 229−233.

(30) Shaw, D. E.; Deneroff, M. M.; Dror, R. O.; Kuskin, J. S.; Larson, R. H.; Salmon, J. K.; Young, C.; Batson, B.; Bowers, K. J.; Chao, J. C.; Eastwood, M. P.; Gagliardo, J.; Grossman, J. P.; Ho, C. R.; Lerardi, D. J.; Kolossváry, I.; Klepeis, J. L.; Layman, T.; McLeavey, C.; Moraes, M. A.; Mueller, R.; Priest, E. C.; Shan, Y.; Spengler, J.; Theobald, M.; Towles, B.; Wang, S. C. Anton, A Special-Purpose Machine for Molecular Dynamics Simulation. *Communications of the ACM* **2008**, *51* (7), 91−97.

(31) Henrion, U.; Renhorn, J.; Borjesson, S. L.; Nelson, E. M.; Schwaiger, C. S.; Bjelkmar, P.; Wallner, B.; Lindahl, E.; Elinder, F. Tracking a Complete Voltage-Sensor Cycle with Metal-Ion Bridges. *Proc. Natl. Acad. Sci. U. S. A.* **2012**, *109*, 8552−8557.

(32) Gandhi, C. S.; Isacoff, E. Y. Molecular Models for Voltage Sensing. *J. Gen. Physiol.* **2002**, *120*, 455−463.

(33) Devaraneni, P. K.; Komarov, A. G.; Costantino, C. A.; Devereaux, J. J.; Matulef, K.; Valiyaveetil, F. I. Semisynthetic K⁺ Channels Show That the Constricted Conformation of the Selectivity Filter is not the C-type Inactivated State. *Proc. Natl. Acad. Sci. U. S. A.* **2013**, *110* (39), 15698−15703.